

Investigating the potential impact of efflorescent mineral crusts on water quality: complementing analytical techniques with geochemical modelling

Bronwyn CAMDEN-SMITH¹, Raymond H. JOHNSON², Robert RICHARDSON¹, David BILLING¹, Hlanganani TUTU¹

¹*Molecular Sciences Institute, School of Chemistry, University of the Witwatersrand, Johannesburg, South Africa*

²*Crustal Geophysics and Geochemistry Science Center, U.S. Geological Survey, Denver CO 80225 USA; bronwyn.camden-smith@students.wits.ac.za*

Abstract Efflorescent crusts are a common feature forming on the surface of gold mining sites and tailings storage facilities during the dry season. Their dissolution at the start of the wet season releases an acidic pulse of water rich in metal pollutants. The composition of the crusts is indicative of the water from which they precipitated. This study aimed at assessing the crust formation and dissolution processes that result in episodic changes in receiving water quality. The approach involved characterising the composition of the crusts by analytical techniques (powder X-ray diffraction (PXRD)) and establishing compositional discrepancies by modelling the formation and dissolution processes.

Keywords geochemical modelling, efflorescent crusts, PXRD, forward modelling, reaction paths

Introduction

Since 1886, the Witwatersrand Basin has hosted more than 150 mines which have extracted over 4.5 Gt of ore at an average grade of nine grams of gold per tonne (McCarthy 2006). Waste rock dumps and tailings storage facilities (TSF), often referred to as "slimes dams," are a common sight in the region. There are more than 270 tailings storage facilities that cover an area of 400 km² in the Witwatersrand and Far West Rand (Durand 2012).

Leachates emanating from these sites have been identified as posing problems of pollution in surrounding water systems (Tutu *et al.* 2008). A common feature fingerprinting this pollution is the occurrence of efflorescent mineral crusts that are usually observed around gold mine TSFs, adjacent streams and other water bodies during the dry season. The crusts contain elevated concentrations of metals and are commonly soluble and insoluble sulphates, hydroxysulphates or hydrated oxides (Jambor *et al.* 2000). Their chemical na-

ture varies depending on the reactions prevailing in the source water, *e.g.* acid generation and neutralisation as well as incongruent precipitation and dissolution.

This variation has been observed particularly in the form of multicoloured crusts (Naicker *et al.* 2003). For instance, white crusts usually indicate the presence of calcium (gypsum), pink indicates cobalt or manganese and green indicates nickel or iron (Naicker *et al.* 2003). Yellow salts can indicate the presence of uranium (Naicker *et al.* 2003). Mineral crusts are significantly more soluble than the primary minerals from which they are derived. The quick dissolution of these salts into surface water at the start of a rainy season leads to a spike in the metal concentration and a lower pH of discharging waters (Nordstrom 2011).

Assessing the mineralogy of these crusts and simulating their dissolution and formation helps to understand the underlying processes leading to their variable composi-

tion and subsequently, that of the water in which they dissolve. This is important in identifying and interpreting gaps existing between what analytical techniques can identify and what simulations predict, thus giving a comprehensive characterisation of the crusts. Remediation attempts and strategies can then be planned by using such information.

Materials and methods

Samples were collected from an abandoned tailings footprint during the dry season in 2012. This site hosted a TSF which was partially reprocessed in 2004. However, due to poor management, the facility was abandoned without rehabilitation. This has resulted in uncontrolled leaching of pollutants into an adjacent natural stream. Leachates drain into a pond within the facility and then seep into the stream via shallow groundwater passages (Fig. 1). Efflorescent crusts are a common feature in the capillary fringe of the pond and can also be observed where leachates seep out of the tailings material. Six samples of distinctly differently coloured efflorescent material were collected from the site (Table 1). The efflorescent material was sampled from the vertical edge of the tailings material (as seen in Fig. 1) as well as from the horizontal upper surface of the TSF.

The crusts (50 g) were dissolved in deionised water and transferred to a 1 L volumetric flask, which was then filled to the mark. Solutions were vacuum filtered using 0.1 μm Prima Pes filter paper. In a preliminary experiment, solutions were gravity filtered using a standard Whatman 11- μm pore-sized filter paper. Measurements of pH, oxidation reduction potential (Eh) and electrical conductivity (EC) were taken before and after filtration. A portion of the solution was analysed using inductively coupled plasma-optical emission spectroscopy (ICP-OES) and chemically suppressed ion chromatography (IC). Bottles were left open and the solutions evaporated at 30 °C. Powder X-ray diffraction of the original samples and the evaporation products were



Fig. 1 The edge of an abandoned tailings storage facility with efflorescent crust on the wall

made using a Bruker D2 Phaser desktop diffractometer which was fitted with a cobalt X-ray source and a LynxEye 1-D detector.

Forward geochemical and reaction path modelling using PHREEQC (Parkhurst and Appelo 1999) were applied to trace the dissolution, evaporation and selective precipitation paths of the solutions of these mineral crusts. Complementary programs used include Simile, a system dynamics, object-based modelling software and Berkely Madonna, a differential equation solver software (Muertzfeldt & Massheder 2003; Macey *et al.* 2009).

Results

Dissolution of the crusts generated acidic solutions, with pH between 2.1 (crust 6) and 3.3 (crust 1). Solutions of crusts with a significant iron concentration had higher Eh measurements than the aluminium-dominant solutions. The highest Eh value was 676 mV (crust 6) whereas the lowest Eh value was 511 mV (crust 2). The crusts that had a significant portion of insoluble mass (crusts 3 and 5) had correspondingly lower EC values (6.4 mS and 5.7 mS). Crusts that were mostly fully dissolved had higher EC values (greater than 10 mS).

The IC results revealed that the solutions of dissolved crusts were essentially sulphate salts. Crust 2 contained a small percentage of chloride. The metal composition of the dissolved sulphate crusts after filtration through

0.1- μm Prima Pes filter paper was analysed using ICP-OES (Table 1). The mole percentages were calculated as the ratio of the metal of interest to the total analysed metal content. The results are listed as mole percentages of the metal content. Crusts 1, 2, 4, and 5 are predominantly aluminium-magnesium sulphate salts. Crust 3 contained similar portions of aluminium, iron and magnesium. Crust 6, a white crust with a bright green interior, contained a high percentage of iron. Crusts with significant iron concentrations (crusts 3 and 6) correspond to the solutions with the highest Eh and lowest pH.

The preliminary experiment using coarse filter paper revealed the potential presence of trace amounts of bismuth, cerium, iridium, gallium, ruthenium, tantalum, thorium, titanium and vanadium. The quantified results for these elements will not be presented here. There have been accounts of a strong dependence of aluminium content on the pore size of filter paper used as it is possible that colloidal aluminium particles dominate an analysis in which there is actually a low portion of dissolved aluminium (Zhu & Anderson 2002). Coarse filter paper was used in the preliminary experiment, and the possibility that these metals were adsorbed on the surface of the colloidal aluminium minerals and not incorporated into the efflorescent crust must not be excluded.

Evaporation modelling of the 0.1- μm filtered solutions of dissolved crusts was undertaken using PHREEQC with the current wateq4f.dat and llnl.dat databases that are provided with the program. The activity models used in these databases are based on the theory of ion dissociation and incorporate modi-

fied Debye-Hückel equations. During evaporation, the ionic strength of the solution increases and the validity of these models decreases. The Pitzer approach, a semi empirical method which uses the theory of ion interaction, would be a more appropriate choice for calculating the activity of the concerned species given the high ionic strength of the solutions towards the end of the evaporation process (Pitzer 1973). Unfortunately, there is a lack of virial coefficients for the system under study. Accornero and Marini (2009) have evaluated the Pitzer parameters for the aluminium species: Al^{3+} , AlOH_2^+ or AlO^+ , with SiO_2 and CO_2 but the parameters for aluminium in an acidic, sulphate-rich system appear to be lacking. In this work, the evaporation has been only modelled up to the point in which the ion-dissociation activity model is valid (an ionic strength of approximately 1 mol kg^{-1}).

Evaporation modelling was approached in a stepwise manner. First, the charge balances and speciation of the solutions were inspected. Second, evaporation of water was modelled with no minerals defined as equilibrium species (Fig. 2). Ideally, minerals of interest should start as undersaturated or close to saturation and become oversaturated during the evaporation of the solution. In the third step, minerals that conform to this requirement are set as equilibrium minerals and are allowed to precipitate when they become oversaturated. In both the wateq4f.dat and llnl.dat databases, none of the aluminium minerals follow this ideal path. Alunite ($\text{KAl}_3(\text{OH})_6(\text{SO}_4)_2$) and jurbanite ($\text{Al}(\text{OH})(\text{SO}_4)$) start as oversaturated whereas the other aluminium minerals remain undersaturated. Aluminium minerals,

Crust	Colour	Al	Ca	Cr	Co	Cu	Fe	K	Mg	Mn	Na	Ni	Tl	Zn
1	Yellow-white	56.9			0.6	0.3		0.6	39.1	1.0		0.9	0.0	0.7
2	Beige	51.4			0.4	0.3	0.3	0.5	43.9	1.2	0.7	0.7		0.6
3	Green-yellow	38.7			0.5	0.9	29.8	2.0	26.6	0.6		0.6		0.4
4	Pink-yellow	50.4		0.1	0.5	0.7	6.6	0.6	38.7	1.0		0.8		0.6
5	Orange-brown	43.6	2.0		0.4	0.5	7.5	1.4	41.7	0.8		0.6	1.0	0.4
6	White with bright green	14.6	0.1	0.1	0.2	0.3	71.9	0.5	11.4	0.3		0.2	0.3	0.1

Table 1 Mole percentages of metals contained in sulphate crusts

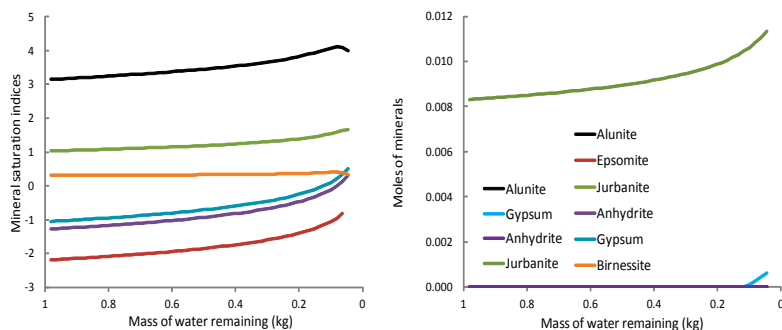


Fig. 2 Modelled saturation indices and precipitation of a selection of minerals during evaporation of dissolved crust solution of Crust 5

such as alunogen ($\text{Al}_2(\text{SO}_4)_3 \cdot 17\text{H}_2\text{O}$), dominate the efflorescent component as seen in the PXRD patterns (Table 2). An exact mineral match is not available in the databases and as such jurbanite and alunite were defined as equilibrium phases. Given that the solutions were exposed to the atmosphere, it was assumed that they are in equilibrium with atmospheric oxygen and carbon dioxide.

The assumption of equilibration of the solution with the atmosphere presented a problem for the crusts that possessed significant iron content. The Eh of these solutions was between 590 and 690 mV. Given the low pH of the solutions, the original iron distribution in these solutions was close to a 1:1 ratio of fer-

rous to ferric ions. Equilibrating the solutions with atmospheric oxygen increases the Eh and the ferric ion dominates. Ferric minerals are thus oversaturated from the beginning of the evaporation modelling. In such cases, the addition of oxygen up to atmospheric conditions was first modelled (Fig. 3) and then followed by the evaporation of water (Fig. 3). The minerals that become oversaturated during the addition of oxygen were selected as equilibrium minerals. Jarosite-H ($(\text{H}_3\text{O})\text{Fe}_3(\text{SO}_4)_2(\text{OH})_6$) was close to saturation at the start of the process and was selected as an equilibrium mineral (Fig. 3). If jarosite-H is not selected as an equilibrium mineral, then amorphous iron hydroxide ($\text{Fe}(\text{OH})_3$) precipitates instead.

Crust	Original	Evaporation products		Geochemical Modelling
		11 µm filtering	0.1 µm filtering	
1	Quartz, alunogen, pickeringite, (bixbyite)	Epsomite, alunogen	None (formed a resin)	Jurbanite, (epsomite close to saturation)
2	Quartz, pickeringite	Pickeringite, alunogen	Pickeringite, alunogen, apjohnite hexahydrate,	Jurbanite, Nsutite (MnO_2), Jarosite-ss (redissolves)
3	Quartz, alunogen	Alunogen, $\text{Al}_2(\text{SO}_4)_3 \cdot 14\text{H}_2\text{O}$	None (formed a resin)	Jarosite-H, jurbanite
4	Quartz, alunogen, pickeringite	None (formed a resin)	None (formed a resin)	Jarosite-K, jarosite-H, jurbanite, nsutite
5	Quartz, alunogen, epsomite	Alunogen, epsomite, hexahydrate	Alunogen, hexahydrate	Gypsum, jurbanite
6	Quartz, coquimbite, magnesiocopiapite	Ferricopiapite, coquimbite, rhomboclase	None (formed a resin)	Jarosite-H, jarosite-K, jurbanite, nsutite

Mineral composition: Alunogen ($\text{Al}_2(\text{SO}_4)_3 \cdot 17\text{H}_2\text{O}$), apjohnite ($\text{MnAl}_2(\text{SO}_4)_4 \cdot 22\text{H}_2\text{O}$), bixbyite (Mn_2O_3), coquimbite ($\text{Fe}_2(\text{SO}_4)_3 \cdot 9\text{H}_2\text{O}$), epsomite ($\text{MgSO}_4 \cdot 7\text{H}_2\text{O}$), ferricopiapite ($\text{Fe}_{4.67}(\text{SO}_4)_6(\text{OH})_2 \cdot 20\text{H}_2\text{O}$), gypsum ($\text{CaSO}_4 \cdot 2\text{H}_2\text{O}$), hexahydrate ($\text{MgSO}_4 \cdot 6\text{H}_2\text{O}$), jarosite-H ($(\text{H}_3\text{O})\text{Fe}_3(\text{SO}_4)_2(\text{OH})_6$), jarosite-K ($\text{KFe}_3(\text{SO}_4)_2(\text{OH})_6$), jarosite-ss ($\text{K}_{0.77}\text{Na}_{0.03}\text{H}_{0.2}\text{Fe}_3(\text{SO}_4)_2(\text{OH})_6$), jurbanite ($\text{Al}(\text{OH})(\text{SO}_4)$), magnesiocopiapite ($\text{MgFe}_4(\text{SO}_4)_6(\text{OH})_2 \cdot 20\text{H}_2\text{O}$), nsutite (MnO_2), pickeringite ($\text{MgAl}_2(\text{SO}_4)_4 \cdot 22\text{H}_2\text{O}$), rhomboclase ($\text{H}_2\text{O}_2\text{Fe}(\text{SO}_4)_2 \cdot 2\text{H}_2\text{O}$)

Table 2 Comparison of original, experimental and predicted mineralogy

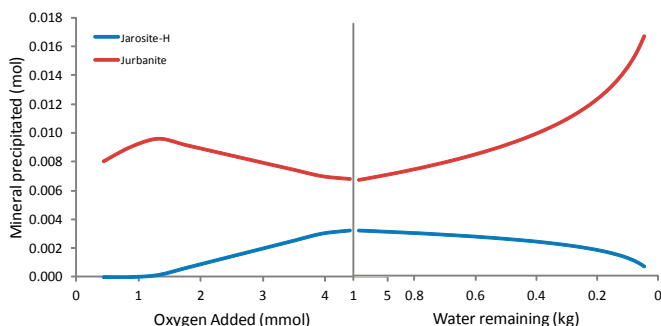


Fig. 3 Modelled precipitation of minerals as a result of addition of oxygen followed by evaporation of dissolved crust solution of Crust 3

The relative rates of evaporation, ferrous oxidation and amorphous iron hydroxide precipitation was investigated by developing a simple systems model in Simile. In this model, a solution containing ferrous and hydronium ions was evaporated. As the solution evaporated, the concentration of the ions increased. The ferrous ions were oxidised to ferric ions. Amorphous iron hydroxide precipitated when the saturation index became positive. This model did not take into account the activity of the ions, but merely their concentration. The modelled rate of evaporation of the solution was fitted to the experimentally observed data with the use of a curve fitting exercise in Berkely Madonna. Literature values for the rate constant of the oxidation of ferrous ions (Singer & Stumm 1970) and the rate constant of precipitation of amorphous iron hydroxide (Grundl & Delwiche 1993) were used. A one-minute time step was used. The 99 % evaporation of a solution which initially contains only ferrous ions and was at an initial pH of 3 was

modelled (Fig. 4). The PHREEQC reaction models assumed equilibration between the ferrous and ferric ions. In relation to a 30 day complete evaporation, the conversion of ferrous ions to ferric ions is slow but the ferric ions quickly precipitate as amorphous $\text{Fe}(\text{OH})_3$ and there are no free ferric ions in solution (Fig. 4). The oxidation of ferrous to ferric ions is known to be a slow process at low pH values (Singer & Stumm 1970), and this kinetic restraint in relation to the rate of evaporation will need to be investigated further for a wider range of minerals.

Table 2 summarises the mineralogy of the crust samples. Predicted minerals do not correlate well with the observed minerals, however the PXRD patterns and the modelling indicate that aluminium minerals are dominant. Thermodynamic data for the minerals observed are not present in the common databases. The geochemical modelling performed in this paper does not take into account factors such as co-precipitation and solid solutions. Both of these factors could cause a mineral to behave differently, in terms of its dissolution and precipitation, to that of the pure end members.

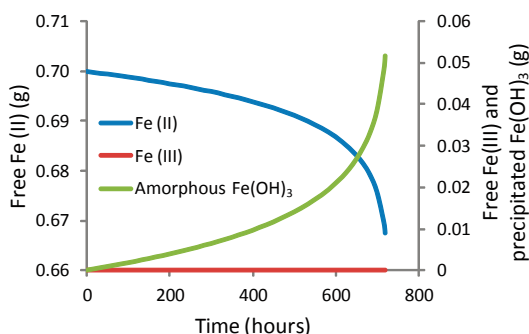


Fig. 4 Simile model of precipitation of amorphous $\text{Fe}(\text{OH})_3$ during evaporation of water

Conclusion

The results of the study indicate the presence of elevated metal concentrations in mineral salt crusts (making them temporary sinks). The efflorescent mineral crusts are readily soluble and mostly generate acidic solutions when dissolved. With additional rainfall and low pH conditions, these pollutants become mobile and can potentially degrade surface

water quality. Geochemical modelling provided more insight into the reactions that occur during formation of the crusts; for instance, the modelling revealed the complexity posed by Eh that causes jarosite precipitation. This complexity derives from the kinetics of Fe precipitation and may help explain why jarosite is predicted to precipitate in geochemical models, but is not observed in the PXRD patterns. However, coquimbite and ferricopiapite were detected in the PXRD patterns and these minerals are paragenetically linked to jarosite. Further, evidence of the need to update most geochemical databases in order to model some of the components became more apparent; for instance, although Al and sulphate appear to be most important, modelling of processes involving them presented a challenge due to the inadequacies of most common databases. Discrepancies between minerals determined analytically and through modelling highlighted the need to use these techniques in a complementary fashion.

Acknowledgements

The authors thank the South African National Research Foundation for funding; the USGS Crustal Geophysics and Geochemistry Science Center for their assistance; the USGS reviewers for their valuable input and the anonymous IMWA reviewer for their helpful comments. Any use of trade, product, or firm names is for descriptive purposes only and does not imply endorsement by the U.S. Government.

References

- Accornero M, Marini L (2009) Empirical prediction of the Pitzer's interaction parameters for cationic Al species with both $\text{SiO}_2(\text{aq})$ and $\text{CO}_2(\text{aq})$: Implications for the geochemical modelling of very saline solutions, *Applied Geochemistry* 24(5), 747–759.
- Durand JF (2012) The impact of gold mining on the Witwatersrand on the rivers and karst system of Gauteng and North West Province, South Africa, *Journal of African Earth Sciences* 68, 24–43.
- Grundl T, Delwiche J (1993) Kinetics of ferric oxyhydroxide precipitation, *Journal of Contaminant Hydrology* 14, 71–97.
- Jambor JL, Nordstrom DK, Alpers, CN (2000) Metal-sulfate Salts from Sulfide Mineral Oxidation, *Reviews in Mineralogy and Geochemistry* 40(1), 303–350.
- Macey R, Oster, G, Zahnley T (2009) Berkeley Madonna User's Guide, Department of Molecular and Cellular Biology, University of California, www.berkeley-madonna.com.
- McCarthy TS (2006) The Witwatersrand Supergroup, in *The Geology of South Africa*, Geological Society of South Africa and Council for Geoscience, Johannesburg.
- Muetzelfeldt RI, Massheder J (2003) The Simile visual modelling environment, *European Journal of Agronomy* 18, 345–358.
- Naicker K, Cukrowska E, McCarthy TS (2003) Acid mine drainage arising from gold mining activity in Johannesburg, South Africa and environs, *Environmental Pollution*, 29–40.
- Nordstrom DK (2011) Hydrogeochemical processes governing the origin, transport and fate of major and trace elements from mine wastes and mineralized rock to surface waters, *Applied Geochemistry* 26, 1777–1791.
- Parkhurst DL, Appelo CAJ (1999) User's guide to PHREEQC (Version2)—A computer program for speciation, batch-reaction, one-dimensional transport, and inverse geochemical calculations. U.S. Geological Survey Water-Resources Investigations Report 99–4259, 310 p.
- Pitzer KS (1973) Thermodynamics of electrolytes. Part I: Theoretical basis and general equations., *J. Phys. Chem.* 77(2), 268–277.
- Singer PC, Stumm W (1970) Acidic mine drainage: The rate determining step, *Science* 167(3921), 1121–1123
- Tutu H, McCarthy TS, Cukrowska E (2008) The chemical characteristics of acid mine drainage with particular reference to sources, distribution and remediation: The Witwatersrand Basin, South Africa as a case study, *Applied Geochemistry* 23(12), 3666–3684.
- Zhu C, Anderson G (2002) *Environmental Applications of Geochemical Modeling*, The Press Syndicate of the University of Cambridge, Cambridge, United Kingdom.